

Magnetic proximity effect and interlayer exchange coupling of ferromagnetic/topological insulator/ferromagnetic trilayer

Mingda Li,^{1,2,*} Wenping Cui,³ Jin Yu,^{1,4} Zuyang Dai,⁵ Zhe Wang,¹ Ferhat Katmis,^{2,6} Wanlin Guo,⁴ and Jagadeesh Moodera^{2,6,†}

¹*Department of Nuclear Science and Engineering, Massachusetts Institute of Technology,
77 Massachusetts Avenue, Cambridge, Massachusetts 02139, USA*

²*Francis Bitter Magnetic Lab, Massachusetts Institute of Technology, 77 Massachusetts Avenue, Cambridge, Massachusetts 02139, USA*

³*Institut für Theoretische Physik, Universität zu Köln, Zùlpicher Strasse 77, D-50937 Köln, Germany*

⁴*State Key Laboratory of Mechanics and Control of Mechanical Structures,
Nanjing University of Aeronautics & Astronautics, Nanjing 210016, China*

⁵*Department of Physics, Tsinghua University, Beijing 100084, China*

⁶*Department of Physics, Massachusetts Institute of Technology, 77 Massachusetts Avenue, Cambridge, Massachusetts 02139, USA
(Received 30 July 2014; revised manuscript received 7 January 2015; published 23 January 2015)*

The magnetic proximity effect between the topological insulator (TI) and ferromagnetic insulator (FMI) is considered to have great potential in spintronics. However, a complete determination of interfacial magnetic structure has been highly challenging. We theoretically investigate the interlayer exchange coupling of two FMIs separated by a TI thin film, and show that the particular electronic states of the TI contributing to the proximity effect can be directly identified through the coupling behavior between two FMIs, together with a tunability of the coupling constant. Such an FMI/TI/FMI structure not only serves as a platform to clarify the magnetic structure of the FMI/TI interface, but also provides insights in designing the magnetic storage devices with ultrafast response.

DOI: [10.1103/PhysRevB.91.014427](https://doi.org/10.1103/PhysRevB.91.014427)

PACS number(s): 75.70.Cn, 73.40.—c

I. INTRODUCTION

The breaking of time-reversal symmetry (TRS), which opens up a gap to the helical Dirac surface states in a three-dimensional strong topological insulator (TI), has been shown to be of central importance for both fundamental aspects [1–8] and device applications [2,6,7,9–12] in TI studies. For instance, the topological magnetoelectric effect [7], which enables the possibility of an electric-field-controlled spin transistor [11,13], requires an opening of the surface band gap as a prerequisite to reach “off” state, otherwise the gapless surface state would lead to a leakage current and very low on/off ratio. Another promising example is the realization of the quantum anomalous Hall effect [14–17], where gapped surface states are accompanied with backscattering-protected edge transport channels without external magnetic field. This opens up the possibility for developing next-generation low-dissipation spintronic devices. Moreover, domain-wall Majorana bound states are predicted at the TI/FMI interface where magnetization switches sign, which could be applied in error-tolerant topological quantum computation [6,7,18]. All the examples above require a gap-opening of the surface states of TI.

In general, there are two approaches to break the TRS and open up the gap: magnetic doping [14–16,19] and magnetic proximity effect [9,15,20–25]. Compared to the doping method, the advantages of the second of these include better controllability of the electronic states, uniformly distributed band gap in space, preservation of the TI’s original crystalline structure, and so on. In this regard, a comprehensive understanding of the interfacial magnetic structure between TI

and FMI becomes essential for observing the above-predicted phenomena.

However, a complete determination of the magnetic structure between TI and FMI turns out to be nontrivial. On the one hand, the interaction between the TI and FMI states is self-consistent in nature, where TI states can lead to complex spin structure, such as magnetic precession in FMI [26]. On the other hand, it is also hindered by the insufficient information experiments that can extract for a comprehensive understanding. For instance, despite the powerful technique of spin-resolved angle-resolved photoemission spectroscopy (ARPES) to study the surface electronic and magnetic structure of doped TI [27] due to the small (~ 1 nm) escape depth of the photoelectrons [28], ARPES renders to be inapplicable to study interfacial magnetic structure where a FMI layer is epitaxially grown on the top of TI. The magneto-optical Kerr effect (MOKE) is another promising method, which could be used to determine both in-plane and out-of-plane magnetization, and has been successfully applied in TI studies [9]. However, the resulting signal of rotated polarization is indeed an overall effect of total magnetization projection, without sensitivity to the individual layer. Due to the short-range nature of exchange coupling [29–35], only the thin layer of magnetic moments very close to the interface contributes to the proximity effect, instead of the total measured magnetization as in MOKE. Actually, at the interface of the TI/FMI structure, strong spin-orbit coupling may tilt the interfacial magnetic moment and result in a different magnetic structure near the interface [20,36]. Another powerful characterization tool is polarized neutron reflectometry (PNR), which has shown great advantages [37] thanks to both compositional and depth sensitivity, but PNR only measures the in-plane magnetization component, without resolving the electronic states of TI which participate in the proximity exchange coupling. Therefore, a deeper understanding of TI/FMI proximity, which considers only the near-interface FMI states, with the distinguishability

*mingda@mit.edu

†moodera@mit.edu

of particular TI states involved in the exchange-coupling process, is clearly needed.

In this study, we calculate the interlayer coupling constant between two thin layers of FMI, separated by a thin spacer layer of three-dimensional TI, within linear response theory [38] and the indirect exchange interaction scheme, which is Ruderman-Kittel-Kasuya-Yosida (RKKY) type interaction [32,35] when the system is conducting, and superexchange interaction when the system is insulating. We take EuS/Bi₂Se₃/EuS as an example of the FMI/TI/FMI trilayer due to the large magnetic moment of the Eu²⁺ ion [39]. Since both the interlayer magnetic coupling and magnetic proximity effect share the same physical origin of exchange coupling between FMI and TI, the TI electronic states participating in the proximity effect are naturally expected to be resolved through the interlayer coupling process.

We use one atomic layer thickness of the magnetic moment of FMI to describe the short-range exchange coupling interaction, and apply the model Hamiltonian of Bi₂Se₃ [1,40] as the prototype of TI. Despite the fact that density functional theory calculation [41,42] shows more complicated behavior, such as the coexistence of the normal and topological surface state, the model Hamiltonian approach is still instructive due to the insights of magnetic coupling it captures, the simplicity when varying the system geometry with no need to build multiple supercells, and is especially useful for nonepitaxial heterostructure where the supercell could not be built. In this approach, we show that a ferromagnetic-antiferromagnetic oscillatory coupling also exists when varying the number of the quintuple layer (QL) of TI, similar to the interlayer exchange coupling results in Fe/Cr/Fe [32,43]. Most importantly, we show distinct behaviors of coupling between the massive Dirac TI state and the p_z bands of Bi and Se due to the paramagnetic nature of Dirac surface state and large diamagnetism of Bi [44,45] orbitals. The sign difference and the tunability of coupling constant vs Fermi level can be applied independently to identify the TI states contributing to the proximity effect due to the same origin of the short-range magnetic exchange coupling process. Our approach, when applied to various FMI/TI/FMI systems, can be used to better understand the TI/FMI proximity effects, and thus for optimized designing of TI-based spintronic devices.

II. THEORY

A. Interlayer exchange coupling constant

Traditionally, the interlayer exchange coupling applies to a trilayer structure where the simple metal or single-atomic species thin layer is sandwiched by two FMIs [29–32]. On the other hand, here TI is a binary compound composed of a quintuple-layered structure. However, even in its original version of interlayer coupling, the single atomic layer is not regarded as real “chemically active” atoms, but instead as a smallest unit of charge density distribution. This allows us to directly generalize it to composite materials from a perspective of coarse-graining. In the present situation of TI, 1 QL, which holds strong chemical binding, could be regarded as the smallest unit, in that the valence and conduction states, which we are interested in, extend over the entire

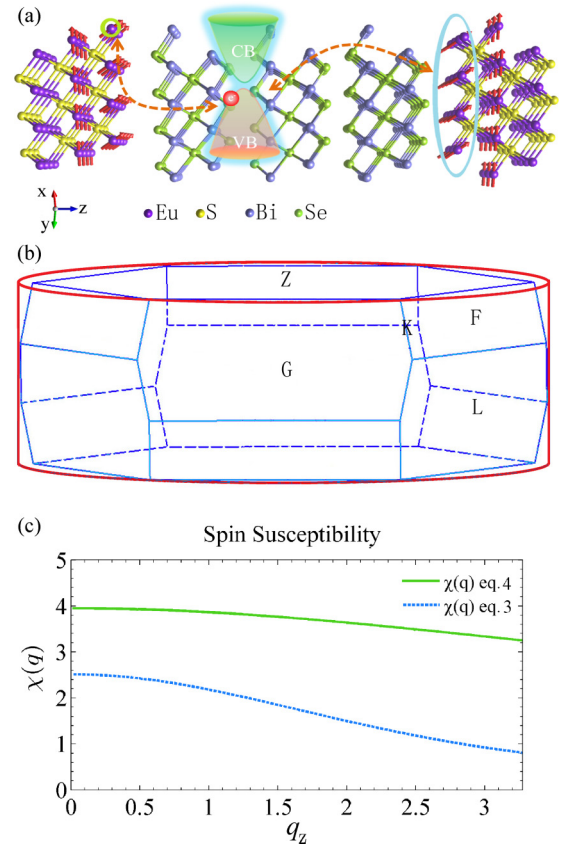


FIG. 1. (Color online) (a) The atomic configuration of EuS/Bi₂Se₃/EuS trilayer, which is a viable example for FMI/TI/FMI structure. The magnetic moment of Eu atoms are shown as red arrows. The spin structure near the interface may be canted near the interface. The interlayer coupling (orange dashed line) is achieved through the electronic states of the TI spacer. (b) The original first Brillouin zone and the simplified cylindrical integration volume. (c) The comparison between spin susceptibilities using Eqs. (3) and (4), with four-band Hamiltonian.

QL. In addition, from the view of the renormalization group, this coarse-graining procedure simply shifts the real-space cutoff from 1 atomic layer to 1 QL. The FMI/TI/FMI trilayer EuS/Bi₂Se₃/EuS is schematically represented in Fig. 1(a). This structure is an important prototype that has been extensively studied [20,39,42,46], while our model is actually generic and not only restricted to this EuS magnet. For a given localized magnetic ion (the Eu ion in the green circle) of FMI close to the interface, the interlayer magnetic coupling constant I_{12} is an overall effect of the indirect exchange coupling of all the Eu ions (blue ellipse) on the other side of the TI/FMI interface, through the coupling of electronic states in TI (orange dashed lines). Due to the localized nature of Eu moments, we could apply the RKKY type of interlayer coupling strength [32,34,35],

$$I_{12} = -\frac{A^2 S^2 d}{2V_0^2 (2\pi)^3} \int dq_z d^2 q_{\parallel} e^{iq_z z} \chi(q_{\parallel}, q_z) \sum_{R_{\parallel} \in F_2} e^{iq_{\parallel} \cdot R_{\parallel}}, \quad (1)$$

where A is the amplitude of the contact potential $A \bar{S}_i \cdot \bar{s}$, with \bar{S}_i and \bar{s} the spins of FMI and TI, respectively, V_0 is the atomic

volume, S is the spin of the FMI, for Eu^{2+} , $S = 7/2$ at 0 K. For finite temperature T , in a mean-field framework we can estimate S as $S(T) = S(0)(1 - (T/T_c)^2)$ for EuS $T_c = 16.6$ K. d is the distance between adjacent atomic planes in its original expression, in our present situation, due to the layered structure of Bi_2Se_3 , it is appropriate to take $d \sim 0.96$ nm, which is the thickness of 1 QL, since 1 QL is the smallest coarse-grained unit for electronic properties, even though 3 QL is the unit for periodic crystalline structure; z is the distance between two FMI layers, $z = (N + 1)d$, where N is the number of QL; R is the in-plane components of the coordinates of the Eu ions to be summed up; and $\chi(q_{\parallel}, q_z)$ is the q -dependent magnetic susceptibility of the TI spacer. The TI states participating in the exchange coupling enter into the $\chi(q_{\parallel}, q_z)$ term, and are finally reflected in I_{12} . This is the theoretical basis why we could study the TI/FMI proximity effect by studying the interlayer coupling of FMI/TI/FMI.

In Eq. (1), the integration of q should be performed within the first Brillouin zone of Bi_2Se_3 [Fig. 1(b), blue polyhedron]. However, if we define q and k periodically in the reciprocal lattice by using a periodic zone scheme instead of a folded zone scheme, we could define a prismatic auxiliary zone and use the reciprocal unit cell with prismatic shape. Since the in-plane area is hexagonal and close to a circle, we further define a cylindrical integration zone which shares the same volume with the original first Brillouin zone [Fig. 1(b), red cylinder], which effectively reduces the integration dimension. Finally, the interlayer coupling constant can be simplified as

$$I_{12} = -\frac{1}{2} \left(\frac{A}{V_0} \right)^2 \frac{S^2 d^2}{2\pi V_0} \int_{-\pi/d}^{+\pi/d} dq_z \chi(q_{\parallel} = 0, q_z) e^{iq_z z}. \quad (2)$$

Here we have used the fact that in the period zone scheme, the in-plane and out-of-plane components are decoupled; for $q_{\parallel} \neq 0$, we have $\sum_{R_{\parallel} \in F_2} e^{iq_{\parallel} \cdot R_{\parallel}} = 0$.

B. q -dependent spin susceptibility

To calculate the interlayer coupling constant I_{12} in Eq. (2), we need the magnetic susceptibility. The spin magnetic susceptibility along direction μ ($\mu = x, y, z$) $\chi_{\mu\mu, \text{spin}}$ for a generic spinor state can be written using the Kubo formula as [47]

$$\chi_{\mu\mu, \text{spin}}(\mathbf{q}) = \frac{\mu_B^2}{4\pi^3} \sum_{\substack{m, \text{occ} \\ n, \text{empty}}} \int d^3\mathbf{k} \frac{f_0(E_{n,\mathbf{k}}) - f_0(E_{m,\mathbf{k}+\mathbf{q}})}{E_{m,\mathbf{k}+\mathbf{q}} - E_{n,\mathbf{k}} + i\delta} \times |\langle m, \mathbf{k} + \mathbf{q} | S_{\mu} | n, \mathbf{k} \rangle|^2, \quad (3)$$

where $E_{n,\mathbf{k}}$ denotes the eigenvalue at band number n and wave vector \mathbf{k} , with corresponding eigenstate $|n, \mathbf{k}\rangle$, S_{μ} ($S_z = I \otimes \sigma_z$, $S_x = \tau_z \otimes \sigma_x$ and $S_y = \tau_z \otimes \sigma_y$) is the spin operator along direction μ and μ_B is the Bohr magneton. The integration over \mathbf{k} is over the cylindrical integration zone in Fig. 1(b).

When the spinor structure is absent, and within the plane-wave approximation, Eq. (3) can be greatly simplified

as [38,48]

$$\chi_{\text{spin}}(\mathbf{q}) = \frac{\mu_B^2}{4\pi^3} \sum_{\substack{m, \text{occ} \\ n, \text{empty}}} \int \frac{f_0(E_{n,\mathbf{k}}) - f_0(E_{m,\mathbf{k}-\mathbf{q}})}{E_{m,\mathbf{k}-\mathbf{q}} - E_{n,\mathbf{k}} + i\delta} d^3\mathbf{k}, \quad (4)$$

where f_0 is the Fermi-Dirac distribution function.

The comparison between Eqs. (3) and (4) is shown in Fig. 1(c). The resulting spin susceptibility [calculated using Eq. (3) and the overlap of eigenstates of Hamiltonian Eq. (7)] is $\sim 1/2$ compared to the result using the simplified version Eq. (4). This could be understood as a consequence of the spin texture of bands, where the electronic transition amplitude for minority spin components is suppressed due to the lack of population in $\sim 1/2$ of the k space [49]. Actually, to calculate the exact magnitude of susceptibility, the density-functional perturbation theory method that requires the input of realistic states and the summation over all bands is needed [50]. However, since we are more interested in the role that the TI state plays in the proximity effect, in addition the effective Hamiltonian approach we adopt involves only a few bands, in the following we use Eq. (4) instead of Eq. (3) to calculate the interlayer coupling constant in Eq. (2), for computational simplicity but without loss of qualitative illustration.

C. Estimation of orbital magnetic susceptibility

Besides the spin susceptibility that contributes to paramagnetism due to the diamagnetic nature of bulk Bi_2Se_3 , we include the diamagnetic orbital term as well. The q -dependent orbital susceptibility can be regarded as an overlap between eigenstates and their curvatures [45,48,50]. In the $q \rightarrow 0$ limit, the susceptibility from spin paramagnetism and orbital diamagnetism can be simplified as [38]

$$\chi_{\text{orb}}(q \rightarrow 0) = -\frac{4}{3} \left(\frac{m_e}{m^* g^*} \right)^2 \chi_{\text{spin}}(q \rightarrow 0), \quad (5)$$

where m^* is the effective mass of electron, $D(E)$ is the density of state near energy E . Despite that in the one-electron theory the linear dispersion seems to result in massless electron $m^* = 0$, in fact the many-body effect, such as electron-phonon coupling, leads to a small but finite m^* [51]. Actually, for the case of the Dirac state, $g^* \simeq \frac{2m_e}{m^*}$ is valid [52], hence we expect the spin paramagnetism to be dominant for Dirac states. This is consistent with the recent experimental report about paramagnetic Dirac susceptibility in TI [53]. On the contrary, for bulk parabolic-like bands $g^* \simeq 2$ [38]. Due to the small effective mass of Bi_2Se_3 , we expect the orbital diamagnetism dominates the spin paramagnetism in bulk Bi_2Se_3 , which is also true based on the experimental value [54]. Neglecting the Van Vleck paramagnetism, which is only significant at high temperature [38], the total magnetic susceptibility at low temperature can be written as

$$\chi(\mathbf{q}) \simeq \chi_{\text{orb}}(\mathbf{q}) + \chi_{\text{spin}}(\mathbf{q}). \quad (6)$$

D. Four-band model Hamiltonian of TI Bi_2Se_3

To calculate the magnetic susceptibility in Eq. (6), eigenvalues from a model Hamiltonian are needed. Due to the hybridization effect between the upper the lower surfaces, the

Hamiltonian is a function of the layer thickness with different hybridization gaps [46]. However, for qualitative demonstration purposes, we take a layer-independent Hamiltonian for simplicity. Using a four-band $k \cdot p$ theory, and a basis $|p_{1z}^+, \uparrow\rangle$, $|p_{2z}^-, \uparrow\rangle$, $|p_{1z}^+, \downarrow\rangle$, $|p_{2z}^-, \downarrow\rangle$, the model Hamiltonian of a TI in Bi_2Se_3 family can be written as [22,40]

$$H(k) = \varepsilon_0(k)I_{4 \times 4} + M(k)I \otimes \sigma_z + A_1 k_z \sigma_z \otimes \tau_x + A_2 k_x \sigma_x \otimes \tau_x - A_2 k_y \sigma_y \otimes \tau_x, \quad (7)$$

where $\varepsilon_0(k) = C + D_1 k_z^2 + D_2(k_x^2 + k_y^2)$, $k_{\pm} = k_x \pm i k_y$, $M(k) = M_0 - B_1 k_z^2 - B_2(k_x^2 + k_y^2)$. For Bi_2Se_3 we have $C = -0.0068 \text{ eV}$, $D_1 = 0.013 \text{ eV} \cdot \text{nm}^2$, $D_2 = 0.196 \text{ eV} \cdot \text{nm}^2$, $M_0 = 0.28 \text{ eV}$, $B_1 = 0.10 \text{ eV} \cdot \text{nm}^2$, $B_2 = 0.566 \text{ eV} \cdot \text{nm}^2$, $A_1 = 0.22 \text{ eV} \cdot \text{nm}$, and $A_2 = 0.41 \text{ eV} \cdot \text{nm}$. The doubly degenerate eigenvalues can be written as

$$E(2_{z,\uparrow/\downarrow}^-, k) = \varepsilon_0(k) + \sqrt{M^2(k) + A_1^2 k_z^2 + A_2^2(k_x^2 + k_y^2)},$$

$$E(1_{z,\uparrow/\downarrow}^+, k) = \varepsilon_0(k) - \sqrt{M^2(k) + A_1^2 k_z^2 + A_2^2(k_x^2 + k_y^2)}, \quad (8)$$

where 1 = Bi and 2 = Se in this notation.

E. Effective Hamiltonian for massive Dirac surface states

Contrary to the four-band model that describes the bulk highest valence and lowest conduction states of Bi_2Se_3 , the surface states are ideally only localized on the TI surface. However, due to the band bending effect that allows surface-state confinement near the interface, multiple surface states penetrate into the bulk [55], including the energetically low-lying Dirac surface states, M-shaped valence states, and Rashba-split conduction states. The strong band bending effect in Bi_2Se_3 can result in a deep penetration of states ~ 12 QL. Thus, for thin TI spacer, it is still important to consider the possibility that the surface states participate in the interlayer magnetic coupling.

For the purpose of qualitative demonstration, we neglect the M-shaped valence states and Rashba-split conduction states, but only keep the Dirac states. The effective Hamiltonian for the Dirac states with gap opening can be written as [1]

$$H_{2D}(k) = Dk^2 I + \begin{pmatrix} \mathcal{H}_D + M \cdot \sigma & tI \\ tI & -\mathcal{H}_D + M \cdot \sigma \end{pmatrix}, \quad (9)$$

where $\mathcal{H}_D = \hbar v_F(\sigma_x k_y - \sigma_y k_x)$. For 4 QL Bi_2Se_3 and magnet MnSe, $M = 28.2 \text{ meV}$, $t = 17.6 \text{ meV}$, $D = 0.098 \text{ eV} \cdot \text{nm}^2$, $v_F = 2.66 \times 10^5 \text{ m/s}$. For a different number of layers, the hybridization t will change accordingly, accompanied with a slight difference of Fermi velocity v_F . For a semiquantitative demonstration purpose, we keep these parameters fixed when varying the thickness of TI and the type of magnet. The eigenvalues can be written as

$$E(k) = Dk^2 \pm \sqrt{\hbar^2 v_F^2 k^2 + M^2 + t^2 + 2\sqrt{M^2 t^2 + \hbar^2 v_F^2 (M_x k_y - M_y k_x)^2}}. \quad (10)$$

In sum, the interlayer coupling constant I_{12} can be thus be calculated by substituting Eq. (6) back to Eq. (2). The eigenvalues in Eqs. (10) and (8) can be used to obtain the magnetic

susceptibility based on Eq. (4). From the modeled Hamiltonian approach since we are more interested in a qualitative behavior rather than a quantitative magnitude, we regard Eq. (5) valid at finite q values to incorporate the orbital contribution.

III. RESULTS AND DISCUSSIONS

The interlayer coupling constant I_{12} as a function of QL number and temperature are shown in Fig. 2, using the bulk four-band Hamiltonian [Eq. (7), Fig. 2(a)] and Dirac Hamiltonian [Eq. (9), Fig. 2(b)]. It is remarkable to see that at the same QL number, a sign difference of I_{12} exists when the interlayer coupling are contributed by the valence and conduction electrons or massive Dirac electrons. This is not only physically reasonable due to the diamagnetic nature of

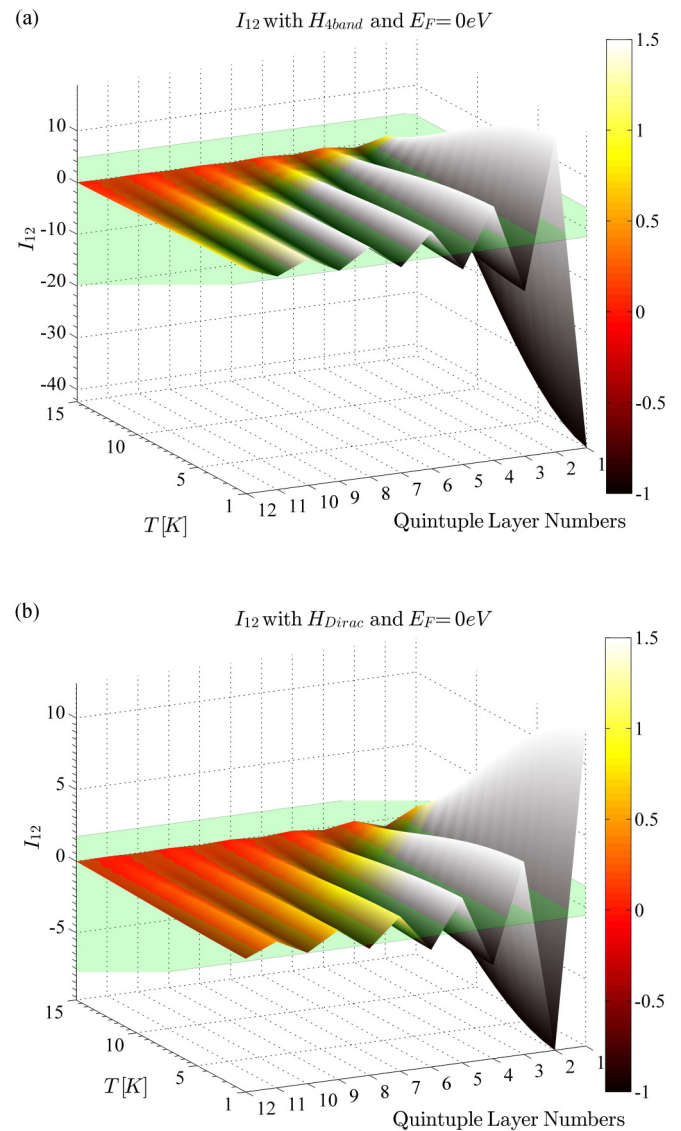


FIG. 2. (Color online) The interlayer exchange coupling constant I_{12} as a function of temperature and number of QL, with (a) four-band Hamiltonian and (b) massive Dirac Hamiltonian. The oscillating ferromagnetic ($I_{12} < 0$) antiferromagnetic ($I_{12} > 0$) coupling behavior is shown in both cases, but with a sign change.

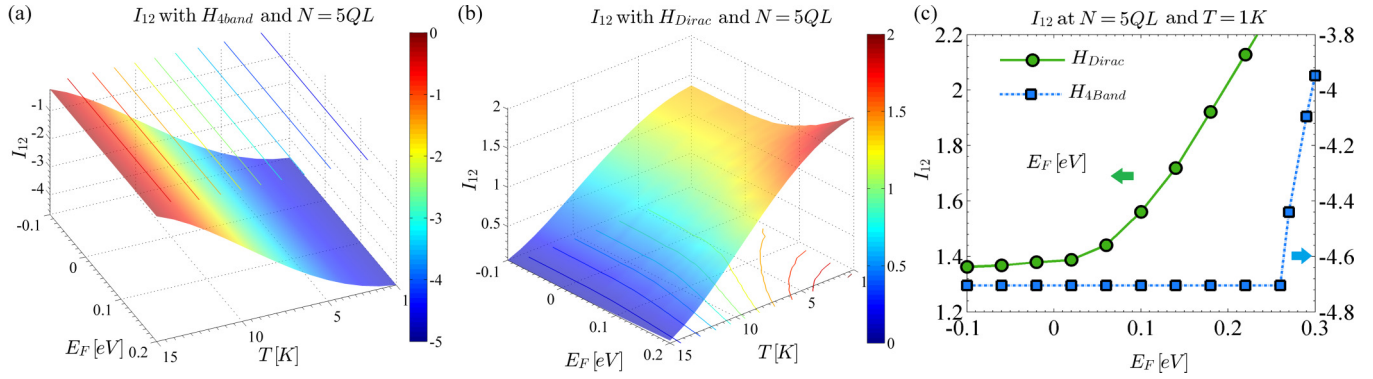


FIG. 3. (Color online) (a, b) Interlayer coupling constant I_{12} at $T = 1$ K, as a function of temperature and Fermi level, for the four-band and Dirac Hamiltonian, respectively. Within the bulk-band gap, I_{12} does not change for the four-band Hamiltonian, while I_{12} is sensitive to E_F for the Dirac Hamiltonian. (c) The comparison of interlayer coupling constant I_{12} between four-band Hamiltonian and Dirac Hamiltonian, at 5 QL and 1 K. We see that for the four-band Hamiltonian I_{12} remains constant while for Dirac Hamiltonian I_{12} keeps changing. This fact can be used to identify the TI states participating in the proximity effect. We can also see that above the bulk band gap, the four-band I_{12} starts to change dramatically.

bulk Bi_2Se_3 and paramagnetic nature of the surface states, but also agrees with the recent experimental report [45] which is able to extract the paramagnetic Dirac susceptibility in the diamagnetic background in TI.

The significance of the sign difference can hardly be overestimated. In device application using the TI/FMI proximity effect, it requires the exchange coupling of FMI with the Dirac surface states to open up the surface band gap. However, the FMI may also couple with other TI states simultaneously. Thus, the sign of I_{12} would tell directly which TI states would dominate the proximity exchange coupling, and provide guidelines to suppress the proximity effect with other TI states while keeping the Dirac surface states dominant for future device design. Moreover, with the aid of the external magnetic field, it is theoretically possible to resolve the relative weights of the coupling strength from the TI Dirac state and other states since they have different responses to the external magnetic field.

Besides the sign change, the dependence of the Fermi level provides further evidence to identify the TI states involved in the proximity effect [Figs. 3(a) and 3(b)]. We see that for the bulk p_z bands [Fig. 3(a)], I_{12} is insensitive with Fermi level E_F within ~ 0.3 eV bulk band gap [Fig. 3(c), blue square curve], whereas on the contrary, a sensitive change of I_{12} with E_F [Figs. 3(b) and 3(c), green circle curve] is shown when coupled with the Dirac states. Therefore, by varying the Fermi level and measuring the variation of I_{12} , it is in principle possible to resolve the particular TI states contributing to the exchange coupling, and determine the relative weights in the proximity effect as well.

Due to the oscillating coupling behavior of nearby QL number, the thickness fluctuation becomes one factor that makes the resulting I_{12} deviate from the ideal case, and hinders further extraction to determine the weights in the proximity effect. In the condition that the lateral correlation length is large enough ($\xi > z$), the averaged effect coupling constant \bar{I}_{12} can be written as averaging over the thickness fluctuations [30]

$$\bar{I}_{12} = \int dz P(z) I(z), \quad (11)$$

where $P(z)$ is the distribution function of spacer thickness. For simplicity we define the Gaussian distribution

$$P(z) = \frac{1}{\sqrt{2\pi}\sigma} \exp\left(-\frac{(z - \bar{z})^2}{2\sigma^2}\right), \quad (12)$$

where σ is the thickness variation. Since the Se-Bi-Se-Bi-Se atomic layers within 1 QL is the strong chemical bonding, while the bonding between QLs is weaker van der Waals interaction, we still use 1 QL as the unit of thickness and discretizing $z \propto d$ with d the thickness of 1 QL, without considering the possibility to break the chemical bonds within 1 QL which leads to fractional thickness in the unit of 1 QL. However, σ can still be arbitrary as it denotes the relative weights for different thicknesses to appear in the layered structure. As an illustration, the resulting change of I_{12} for the four-band Hamiltonian with different σ is shown in Fig. 4. When the thickness fluctuation increases, the

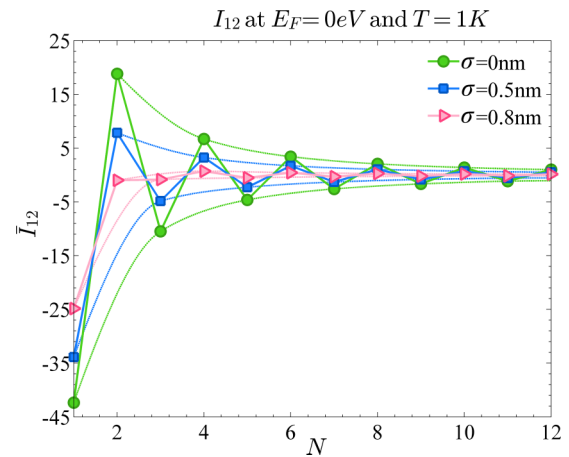


FIG. 4. (Color online) The interlayer coupling constant I_{12} at various thickness fluctuation, $\sigma = 0.5$ and 0.8 nm, using a four-band Hamiltonian model at $E_F = 0$ eV and $T = 1$ K. Stronger thickness fluctuation has a smoothing effect on the overall coupling constant, and may hamper the manifestation of TI states participating in the proximity effect.

resulting averaged \bar{I}_{12} drops dramatically. Thus, to determine the particular TI states involved in the proximity exchange coupling as well as their relative weights, high-quality samples with negligible thickness fluctuation are desirable.

IV. CONCLUSION

We have provided a systematic approach to illustrate the feasibility that how interlayer exchange coupling in FMI/TI/FMI structure can help understand the TI/FMI proximity effect, with the capability to identify the TI states involved in the proximity exchange. By changing the external magnetic field or Fermi level, the weights for the exchange coupling between the FMI and desired TI Dirac states can be obtained. Such information can hardly be obtained directly by the experimental probes such as ARPES, MOKE, PNR, or transport since this approach circumvents the complications of the TI-FMI interaction, but infers the TI states from the simpler indirect FMI-FMI coupling using TI states as medium. In this perspective, the interlayer coupling between two FMIs in the FMI/spacer/FMI structure is not only an interesting phenomenon by itself, but also can be regarded as a probe to study the properties of the spacer.

Moreover, since the interlayer exchange coupling in magnetic multilayers, such as the Fe/Cr superlattice [56],

has played a significant role in giant magnetoresistance (GMR) [57–59], the present work also sheds light on the application of magnetic data storage and magnetic field sensors. As shown in Fig. 3(c), the interlayer exchange coupling constant could be tuned when coupling with Dirac states of TI. This provides a method to achieve electrically controlled magnetic coupling, with reversibility due to gating, and rapid response due to high-mobility, backscattering-protected Dirac electrons. The only prerequisite is that the exchange coupling with massive Dirac states should overcome the bulk TI states. This may be realized in thinner TI film where the bulk bands diminish whereas the surface bands dominate. Therefore, further studies of interlayer exchange coupling in TI-based magnetic layers for GMR applications are highly desired.

ACKNOWLEDGMENTS

M.L. would thank Ju Li for generous support and helpful discussions. J.S.M. and F.K. would like to thank support from the MIT MRSEC through the MRSEC Program of the NSF under Award No. DMR-0819762. J.S.M. would like to thank support from NSF DMR Grant No. 1207469 and ONR Grant No. N00014-13-1-0301.

-
- [1] W. Luo and X.-L. Qi, *Phys. Rev. B* **87**, 085431 (2013).
 [2] R. Li, J. Wang, X.-L. Qi, and S.-C. Zhang, *Nat. Phys.* **6**, 284 (2010).
 [3] X.-L. Qi, R. Li, J. Zang, and S.-C. Zhang, *Science* **323**, 1184 (2009).
 [4] Q. Liu, C.-X. Liu, C. Xu, X.-L. Qi, and S.-C. Zhang, *Phys. Rev. Lett.* **102**, 156603 (2009).
 [5] X.-L. Qi, T. L. Hughes, and S.-C. Zhang, *Phys. Rev. B* **78**, 195424 (2008).
 [6] X.-L. Qi and S.-C. Zhang, *Rev. Mod. Phys.* **83**, 1057 (2011).
 [7] M. Z. Hasan and C. L. Kane, *Rev. Mod. Phys.* **82**, 3045 (2010).
 [8] V. N. Men'shov, V. V. Tugushev, S. V. Eremeev, P. M. Echenique, and E. V. Chulkov, *Phys. Rev. B* **88**, 224401 (2013).
 [9] M. Lang, M. Montazeri, M. C. Onbasli, X. Kou, Y. Fan, P. Upadhyaya, K. Yao, F. Liu, Y. Jiang, W. Jiang, K. L. Wong, G. Yu, J. Tang, T. Nie, L. He, R. N. Schwartz, Y. Wang, C. A. Ross, and K. L. Wang, *Nano Lett.* **14**, 3459 (2014).
 [10] X. Li, Y. G. Semenov, and K. W. Kim, in *Device Research Conference (DRC), 2012 70th Annual* (IEEE, New York, 2012), pp. 111–112.
 [11] L. A. Wray, *Nat. Phys.* **8**, 705 (2012).
 [12] I. Vobornik, U. Manju, J. Fujii, F. Borgatti, P. Torelli, D. Krizmancic, Y. S. Hor, R. J. Cava, and G. Panaccione, *Nano Lett.* **11**, 4079 (2011).
 [13] Q.-K. Xue, *Nat. Nanotechnol.* **6**, 197 (2011).
 [14] C.-Z. Chang, J. Zhang, X. Feng, J. Shen, Z. Zhang, M. Guo, K. Li, Y. Ou, P. Wei, L.-L. Wang, Z.-Q. Ji, Y. Feng, S. Ji, X. Chen, J. Jia, X. Dai, Z. Fang, S.-C. Zhang, K. He, Y. Wang, L. Lu, X.-C. Ma, and Q.-K. Xue, *Science* **340**, 167 (2013).
 [15] Q.-K. Xue, *Natl. Sci. Rev.* **1**, 31 (2014).
 [16] J. Wang, B. Lian, H. Zhang, Y. Xu, and S.-C. Zhang, *Phys. Rev. Lett.* **111**, 136801 (2013).
 [17] R. Yu, W. Zhang, H.-J. Zhang, S.-C. Zhang, X. Dai, and Z. Fang, *Science* **329**, 61 (2010).
 [18] B. A. Bernevig, *Topological Insulators and Topological Superconductors* (Princeton University Press, Princeton, NJ, 2013).
 [19] V. N. Men'shov, V. V. Tugushev, and E. V. Chulkov, *JETP Lett.* **94**, 629 (2011).
 [20] P. Wei, F. Katmis, B. A. Assaf, H. Steinberg, P. Jarillo-Herrero, D. Heiman, and J. S. Moodera, *Phys. Rev. Lett.* **110**, 186807 (2013).
 [21] V. N. Men'shov, V. V. Tugushev, and E. V. Chulkov, *JETP Lett.* **98**, 603 (2014).
 [22] A. T. Lee, M. J. Han, and K. Park, *Phys. Rev. B* **90**, 155103 (2014).
 [23] V. N. Men'shov, V. V. Tugushev, and E. V. Chulkov, *JETP Lett.* **97**, 258 (2013).
 [24] V. N. Men'shov, V. V. Tugushev, and E. V. Chulkov, *JETP Lett.* **96**, 445 (2012).
 [25] Z. Jiang, F. Katmis, C. Tang, P. Wei, J. S. Moodera, and J. Shi, *Appl. Phys. Lett.* **104**, 222409 (2014).
 [26] X. Li, X. Duan, and K. W. Kim, *Phys. Rev. B* **89**, 045425 (2014).
 [27] D. Hsieh, Y. Xia, L. Wray, D. Qian, A. Pal, J. Dil, J. Osterwalder, F. Meier, G. Bihlmayer, C. Kane, Y. S. Hor, R. J. Cava, and M. Z. Hasan, *Science* **323**, 919 (2009).
 [28] L. A. Wray, S. Xu, M. Neupane, A. V. Fedorov, Y. S. Hor, R. J. Cava, and M. Z. Hasan, *J. Phys.: Conf. Ser.* **449**, 012037 (2013).
 [29] P. Bruno, *J. Phys.: Condens. Matter* **11**, 9403 (1999).
 [30] P. M. Levy, S. Maekawa, and P. Bruno, *Phys. Rev. B* **58**, 5588 (1998).

- [31] P. Bruno, *J. Magn. Magn. Mater.* **164**, 27 (1996).
- [32] P. Bruno, *Phys. Rev. B* **52**, 411 (1995).
- [33] E. Bruno and B. L. Gyorffy, *Phys. Rev. Lett.* **71**, 181 (1993).
- [34] P. Bruno, *J. Magn. Magn. Mater.* **121**, 248 (1993).
- [35] P. Bruno and C. Chappert, *Phys. Rev. B* **46**, 261 (1992).
- [36] P. Bruno, *Phys. Rev. B* **39**, 865 (1989).
- [37] S. R. Spurgeon, J. D. Sloppy, D. M. Kepaptsoglou, P. V. Balachandran, S. Nejati, J. Karthik, A. R. Damodaran, C. L. Johnson, H. Ambaye, R. Goyette, V. Lauter, Q. M. Ramasse, J. C. Idrobo, K. K. S. Lau, S. E. Lofland, Jr., J. M. Rondinelli, L. W. Martin, and M. L. Taheri, *ACS Nano* **8**, 894 (2014).
- [38] R. M. White, *Quantum Theory of Magnetism: Magnetic Properties of Materials* (Springer, New York, 2007), Vol. 32.
- [39] Q. I. Yang, M. Dolev, L. Zhang, J. Zhao, A. D. Fried, E. Schemm, M. Liu, A. Palevski, A. F. Marshall, S. H. Risbud, and A. Kapitulnik, *Phys. Rev. B* **88**, 081407 (2013).
- [40] C.-X. Liu, X.-L. Qi, H. J. Zhang, X. Dai, Z. Fang, and S.-C. Zhang, *Phys. Rev. B* **82**, 045122 (2010).
- [41] S. V. Eremeev, V. N. Men'shov, V. V. Tugushev, P. M. Echenique, and E. V. Chulkov, *Phys. Rev. B* **88**, 144430 (2013).
- [42] S. V. Eremeev, V. N. Men'shov, V. V. Tugushev, and E. V. Chulkov, [arXiv:1407.6880](https://arxiv.org/abs/1407.6880).
- [43] J. Kienert, Ph.D. thesis, Humboldt University of Berlin, 2008.
- [44] F. Buot and J. McClure, *Phys. Rev. B* **6**, 4525 (1972).
- [45] J. E. Hebborn and N. H. March, *Proc. R. Soc. Lond. A* **280**, 85 (1964).
- [46] F. S. Nogueira and I. Eremin, *Phys. Rev. B* **90**, 014431 (2014).
- [47] L.-P. Levy, *Magnetism and Superconductivity* (Springer, New York, 2000).
- [48] J. Hebborn and N. March, *Adv. Phys.* **19**, 175 (1970).
- [49] O. V. Yazyev, J. E. Moore, and S. G. Louie, *Phys. Rev. Lett.* **105**, 266806 (2010).
- [50] F. Mauri and S. G. Louie, *Phys. Rev. Lett.* **76**, 4246 (1996).
- [51] E. Tiras, S. Ardali, T. Tiras, E. Arslan, S. Cakmakyapan, O. Kazar, J. Hassan, E. Janzn, and E. Ozbay, *J. Appl. Phys. (Melville, NY, US)* **113**, 043708 (2013).
- [52] M. Koshino and T. Ando, *Phys. Rev. B* **81**, 195431 (2010).
- [53] L. Zhao, H. Deng, I. Korzhovska, Z. Chen, M. Konczykowski, A. Hruban, V. Oganessian, and L. Krusin-Elbaum, *Nat. Mater.* **13**, 580 (2014).
- [54] M. Kumar, *Diamagnetic Susceptibility and Anisotropy of Inorganic and Organometallic Compounds* (Springer, New York, 2007), Vol. 27.
- [55] M. Bahrany, P. King, A. De La Torre, J. Chang, M. Shi, L. Patthey, G. Balakrishnan, P. Hofmann, R. Arita, N. Nagaosa, and F. Baumberger, *Nat. Commun.* **3**, 1159 (2012).
- [56] M. N. Baibich, J. M. Broto, A. Fert, F. Nguyen Van Dau, F. Petroff, P. Etienne, G. Creuzet, A. Friederich, and J. Chazelas, *Phys. Rev. Lett.* **61**, 2472 (1988).
- [57] A. Fert, P. Grünberg, A. Barthélémy, F. Petroff, and W. Zinn, *J. Magn. Magn. Mater.* **140-144**, 1 (1995).
- [58] S. S. P. Parkin, N. More, and K. P. Roche, *Phys. Rev. Lett.* **64**, 2304 (1990).
- [59] S. S. P. Parkin, R. Bhadra, and K. P. Roche, *Phys. Rev. Lett.* **66**, 2152 (1991).